Laser-Induced Periodic Surface Structures (LIPSS) on Polymers Processed with Picosecond Laser Pulses

Marek Mezera[1], Martin van Drongelen[2], G.R.B.E. Römer[1]

[1] *Chair of Laser Processing, Department of Mechanics of Solids, Surfaces and Systems (MS³), Faculty of Engineering Technology, University of Twente, 7500 AE, Enschede, The Netherlands*
E-mail: m.mezera@utwente.nl
[2] *Chair of Production Technology, Department of Mechanics of Solids, Surfaces and Systems (MS³), Faculty of Engineering Technology, University of Twente, 7500 AE, Enschede, The Netherlands*

Based on a literature review, it was concluded that Laser-induced Periodic Surface Structures (LIPSS) on polymers are produced when applying laser sources operating either in the ultraviolet wavelength and nanosecond pulse duration, or radiation of wavelengths ranging from 265nm to 1045nm and pulse durations in the femtosecond regime. LIPSS were not reported when using picosecond laser sources. The purpose of this paper is to study whether (and if so which) LIPSS form on polymers when picosecond pulsed laser source is applied. Low Spatial Frequency LIPSS (LSFL) and High Spatial Frequency LIPSS (HSFL) have been obtained on polycarbonate and on polystyrene when applying picosecond laser pulses at a wavelength of 343nm on single spots and on processed lines. When using a wavelength of 515nm, LSFL and HSFL have been produced only on polycarbonate, but also led to porosity of the structured area.
DOI: 10.2961/jlmn.2018.02.0010
Keywords: laser-induced periodic surface structures (LIPSS); low spatial frequency LIPSS (LSFL); high spatial frequency LIPSS (LSFL); Polycarbonate (PC); Polystyrene (PS); picosecond laser source

1. Introduction

Laser induced Periodic Surface Structures (LIPSS) are regular nanoscale structures which develop on top of surfaces when processed with a linear or circular polarized laser beam in a narrow range of fluence levels close to the ablation threshold [1]. LIPSS have been observed on a wide range of materials, such as metals [2–5], semiconductors [2,6–10], dielectrics [2,11–13], ceramics [14] and polymers [15–22]. LIPSS were found first on semiconductors by Birnbaum [6] in 1965. His discovery led to an extensive research on this universal phenomenon [23]. LIPSS come in a wide range of shapes, e.g. ripples [23], pillars [24], grooves and cones [25]. Most researched LIPSS are low spatial frequency LIPSS (LSFL) which are ripples with a distinct orientation, either parallel or perpendicular to the laser polarization (depending on the material) and a spatial periodicity Λ close to the laser wavelength λ [23]. In the early 2000s, when commercial ultra-short pulsed laser sources entered the market, LIPSS with a periodicity Λ much smaller than the laser wavelength λ have been observed ($\Lambda << \lambda$). These LIPSS are referred to as High spatial frequency LIPSS (HSFL) [23]. The properties of these structures (the spatial period and amplitude) are controlled by several laser parameters including the laser wavelength, the type of polarization of the laser light (e.g. linear or circular), the angle of incidence of the laser beam on the surface, the laser fluence, the number of pulses and the geometrical pulse-to-pulse overlap [26].

Table 1 Abbreviations of five polymers, on which LIPSS formation has been mostly reported

Polymer	Abbreviation
Polycarbonate	PC
Polyethylene terephthalate	PET
Polyimide	PI
Polystyrene	PS
Polytrimethylene terephthalate	PTT

Applications for LIPSS on polymers include, e.g. increased cell adhesion and growth on polymer surfaces processed with LIPSS [27–29]; LIPSS on polymers can be used as Surface Enhanced Raman Scattering (SERS) sensors [29–31]; and LIPSS on Poly(3-hexylthiophene-2,5-diyl) (P3HT) changes the conductivity on the surface [29,32,33].
Table 1 lists the five most studied polymers on which LIPSS have been reported in literature. Tables 2,3 and Fig. 1 summarize a literature study on these five polymers. LIPSS on polymers have been reported after irradiating the surface with linear or circular polarized laser beams [29].
In contrast to metals and semiconductors, where LSFL form perpendicular to the laser polarization [2], formation of LSFL on polymers nearly always form parallel to the laser polarization direction, see Table 1. The formation of “normal” LSFL (perpendicular to the laser polarization) and “anomalous” LSFL (parallel to the laser polarization) was investigated numerically and experimentally on a Ti film by Pavlov et. al. [34]. These authors state, that normal LSFL form at a low number of pulses per spot at a fluence level near or above the ablation threshold due to the interference of the incident laser beam with surface plasmon polaritons (SPP’s), which are travelling at the surface perpendicular to the laser polarization and are generated due to near field scattering at surface defects. Anomalous LSFL, on the other hand, form

at high number of pulses at a fluence level significantly below the ablation threshold. The incident laser beam scatters dipole-like in the far-field at all surface defects along the surface, which are smaller than the laser wavelength. The interference of the incident laser beam with the scattered light leads to peak intensities in a pattern parallel to the laser polarization. Since the fluence level is much below the ablation threshold, oxidation occurs at the location of peak intensities. The resulting structures can be extended coherently over a large area (larger than the beam spot size) by scanning the laser beam over the surface. Already created structures from previous pulses act as light scattering sources to create homogeneous structures along the beam path. Therefore, parallel LIPSS on polymers form due to the interference of the incident laser beam with far-field scattering of light.
Further, in contrast to metals, on which LIPSS are formed after single to dozens of laser pulses, it has been found, that to produce LIPSS on polymers with a ns laser source, several hundreds to thousand pulses need to be applied on the same spot on the surface. As a possible explanation for this phenomenon, Rebollar et al. [35] suggested that polymers need to reach the glass transition (T_g) or even the melting temperature (T_m) in order to increase the mobility of the polymer chains for surface modifications. As each subsequent pulse may lead to an increase of the sample (surface) temperature due to heat accumulation, the glass transition or melting temperature may be reached. When applying fs laser pulses to the surfaces of polymers, it is possible to process polarization direction independent LSFL after only 2 pulses, which become more pronounced and oriented parallel to the laser polarization direction after 5 pulses [36]. HSFL have been observed after 100 pulses, also parallel to the laser polarization [18,37].

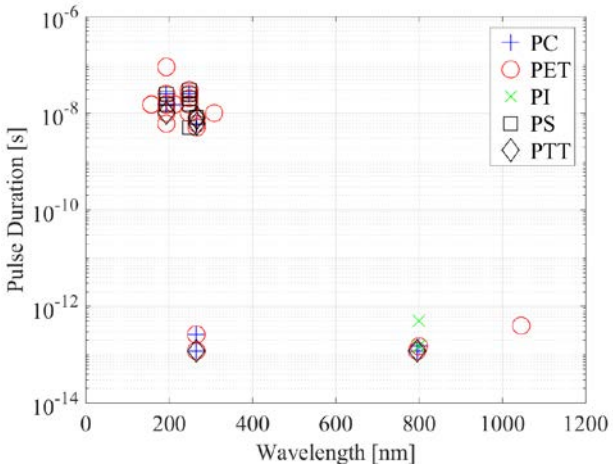

Fig. 1 LIPSS (categorized by laser parameters pulse duration and laser wavelength) on the five polymers on which have been reported the most in literature, see also Table 1, 2 and 3.

From Fig. 1 and Table 1 it can be concluded that most studied report LIPSS formation on polymers using nanosecond (ns) pulsed laser sources operating in the UV wavelength regime. A vast variety of synthetic and natural polymers have high absorptivity in the ultraviolet spectrum. The high amount of energy input of UV radiation (e.g. 150 to 350 nm: 800 – 340 kJ/mole) causes bond breaking of the molecular chains and produces highly reactive radicals which results in a reduction of the molecular weight and changes the mechanical and optical properties of the polymer [42].

Table 2 LIPSS processing parameters for the five most reported polymers on which LIPSS formation was shown in the fs regime

Material	Pulse duration [fs]	Wavelength [nm]	Absorption Coefficient α [cm^{-1}]	Laser Fluence [mJ/cm²]	Laser Frequency [Hz]	Number of Pulses	LIPSS type	Orientation of LIPSS to polarization	References
PC	120	265	1.8e4	1.1-1.4	1000	500-20000	LSFL	parallel	[35]
PC	260	265	1.8e4	1-2.4	1000	5000	LSFL	parallel	[38,39]
PC	120	795	365	35.4-36.2	1000	50000	LSFL	parallel	[38,39]
PET	500	248	1e5	53-59; 79	N/A	5	LSFL	parallel	[18,37]
PET	500	248	1e5	59; 79	N/A	5	HSFL	parallel	[18,37]
PET	120	265	1.8e4	1.1-35	1000	500-50000	LSFL	parallel	[35]
PET	260	265	1.8e4	1-2.4	1000	5000	LSFL	parallel	[38,39]
PET	120	795	835	35.4-36.2	1000	50000	LSFL	parallel	[38,39]
PET film on Si wafer	400	1045	N/A	40-80	100000	100000	LSFL	perpendicular	[40]
PI	500	248	1e5	14	N/A	60	LSFL	parallel	[37]
PI	500	248	1e5	83	N/A	>10	LSFL	parallel and perpendicular	[18]
PI (Kapton; Cirlex)	150-500	800	18; 37	600-1400	1000	2-100	LSFL	parallel	[36]
PI	150	800	N/A	1000-2600	2	50-60	LSFL; Cones	parallel	[41]
PTT	120	265	2.6e4	1.3-1.6	1000	500-20000	LSFL	parallel	[35]
PTT	120	795	705	35-37	1000	50000	LSFL	parallel	[31,35]

Table 3 LIPSS processing parameters for the five most reported polymers on which LIPSS formation was shown in the ns regime

Material	Pulse duration [ns]	Wavelength [nm]	Absorption Coefficient α $[cm^{-1}]$	Laser Fluence [mJ/cm²]	Laser Frequency [Hz]	Number of Pulses	LIPSS type	Orientation of LIPSS to polarization	Reference
PC	15	193	5.5e5	3-5	1-7	400-1000	LSFL	parallel	[43–45]
PC	25	193	5.5e5	3-5.2	1-7	400-2000	LSFL	parallel	[17]
PC	5-7	193	5.5e5	3-5	N/A	1200	LSFL	parallel	[46]
PC	25	248	1e4		1-7	1000	No structures	-	[17]
PET	15	157	2.3e5	3.8-4.7	5	5600	LSFL	parallel	[47]
PET	15	157	N/A	4.4	11	5600	LSFL	parallel	[48]
PET	15	193	3e5	3-5	3	1000	LSFL	parallel	[17]
PET	15	193	3e5	3-5	N/A	1000	LSFL	parallel	[19]
PET	5	193	N/A	3-5	N/A	1200	LSFL	parallel	[46]
PET	10	193	1.6e5	3	4	600	LSFL	parallel	[28]
PET	15	248	1.6e5	4-10.5	3	1000	LSFL	parallel	[17]
PET	15	248	N/A	5	N/A	1000	LSFL	parallel	[19]
PET	20	248	N/A	6.6	11	6000	LSFL	parallel	[48]
PET	20	248	N/A	10.5-12.5	10	6000	LSFL	parallel	[49]
PET	6	266	1.8e4	7	10	300	LSFL	parallel	[39]
PET	5	266	1.8e4	7	10	1200	LSFL; Cones	parallel	[28]
PS	25	193	8e5	3-5	1-7	1000	LSFL	parallel	[17]
PS	20	193	1.67e5	80	10	400	Cones	-	[50]
PS	25	248	6e3		1-7	1000	No structures	-	[17]
PS	30	248	N/A	7.1-8.9	10	6000	LSFL	parallel	[27]
PS	20	248	6.1e3	10	10	6000	LSFL	parallel	[22]
PS	20	248	N/A	10.5-12.5	10	6000	LSFL	parallel	[49]
PS	8	266	1.6e3	10	10	3600-6000	LSFL	parallel	[21]
PTT	8	193	N/A	3	4	600	LSFL	parallel	[31]
PTT	8	266	2.6e4	6	10	300-1200	LSFL	parallel	[51]
PTT	8	266	2.6e4	7	1-10	2000	LSFL	parallel	[52]
PTT	6	266	2.6e4	1-15	10	100-6000	LSFL	parallel	[51]
PTT	8	266	N/A	5-10	10	1200	LSFL	parallel	[20]
PTT	6	266	N/A	7	10	1200	LSFL; Cones	parallel	[31]

Further, LSFL formations is not reported when using wavelengths in the visible or infrared spectra and using ns pulsed laser sources, since the absorptivity of most polymers is too low for these wavelengths. In this case, absorption can only occur at material defects in larger depths, which causes decomposition and gasification in deeper regions whereby any possibility of an ordered structure will be disturbed [36]. Processing LIPSS on polymers with laser sources emitting wavelengths in the visible or infrared spectra is possible when femtosecond (fs) pulsed laser sources are applied, see Table 3 and Fig. 1. In this case the ultrashort pulse durations lead to high peak densities, resulting in non-linear two- and multiphoton absorption and ionization before material relaxation occurs. This opens the possibility to process materials which are transparent at the given laser wavelength without thermal processes, e.g. without an increase of the surface temperature [29]. Rebollar et al. [29] showed, that to produce LIPSS on polymers, the amount of pulses processing the same spot with femtosecond laser pulses need to increase with decreasing fluence levels, as was also shown for ns pulses. This suggests, that some kind of feedback mechanism is involved in the formation of LIPSS [53,54]. The majority of literature listed in Table 2 and 3 focus on the development of LSFL. HSFL have been reported only when processing polymers in the fs regime [18,37]. It is known that, on metals, HSFL generally occur when processing the material with fluence levels close to the ablation threshold in both the femtosecond and picosecond regime [23]. The origin of HSFL formation is still under discussion and several theories are proposed, e.g. self-organization of the excited surface [55], second- and third-harmonic generation [56], oxidation [57] and twinning during the resolidification of a thin laser-induced melt layer [58].

Summarizing it can be concluded from Fig. 1 and Tables 2 and 3, that LIPSS occur on polymers when using laser sources of either ns pulse duration and UV wavelength, or pulse durations in the fs regime at wavelength ranging from 265nm to 1045nm. In contrast, LIPSS on polymers using pulse durations in the picosecond regime have not been reported. The purpose of this paper is to study whether (and, if

so, which) LIPSS form on polymers when a picosecond pulsed laser source is applied.

2. Materials and Experimental Setup

Table 4 Laser processing conditions at a laser pulse frequency of f=1000 Hz

Material	Single Spot		Line (OL~0.9)	
$\lambda = 343$ nm	F [mJ/cm²]	N_{OS}	F [mJ/cm²]	N_{OS}
PS	18 - 167	1 - 5000	7 - 83	500 - 10000
PC	330 - 6972	1 - 7500	7 - 23	500 - 10000
$\lambda = 515$ nm	F [mJ/cm²]	N_{OS}		
PS	11 - 190	1 - 5000		
PC	390 - 1834	1- 5000		

In this work, two types of customary free standing polymers were used:

- A 1.2mm thick white polystyrene (PS) plate consisting of 97% polystyrene (Polybatch 3% white pigment from A. Schulman, USA).
- A 5mm thick polycarbonate (Makrolon GP from Covestro AG, Germany).

The surface roughness of both samples was measured using a confocal microscope (VK9710 of Keyence Corporation, Japan) and found to equal R_z=5.4µm (PC) and R_z=68.6µm (PS). The absorption coefficients are listed below.

Table 5 Absorption Coefficients of PC and PS

Material	Wavelength [nm]	Absorption Coefficient α [cm^{-1}]	Reference
PC	343	45	[59]
PC	515	20	[59]
PS	343	60	[60]
PS	515	40	[60]

A pulsed Yb:YAG disk laser source (TruMicro 5050 of Trumpf GmbH, Germany) with a wavelength of 1030 nm, maximum pulse frequency of 400 kHz, pulse energies up to 125 µJ and a pulse duration of 6.7ps and a nearly Gaussian beam profile ($M^2 \leq 1.3$) was used. The samples were irradiated with two wavelengths, which were generated by a Second Harmonic Generator (SHG, 515nm) and a Third Harmonic Generator (THG, 343nm). The laser beam was focused on the surface of the samples using telecentric F-theta objectives. One objective for 515nm (Ronar of Linos GmbH, Germany) having a focal length of 100mm and one objective for 343nm (JENar of Jenoptic Laser GmbH, Germany) having a focal length of 103mm. The focal $1/e^2$ beam diameters were measured using a laser beam characterization device MicroSpotMonitor of Primes GmbH (Germany) and found to equal 13.2µm and 9.8µm, respectively. The laser beam was scanned over the sample using a galvanoscanner (intelliSCAN14 from ScanLab GmbH, Germany) with an accuracy of 2µrad with mirrors coated for the wavelength used. The laser power was measured using a photodiode power sensor at a measurement uncertainty of ±8% for UV (OP-2 UV from Coherent, Inc, USA) and of ±5% for VIS (OP-2 VIS from Coherent, Inc, USA) connected to a readout unit (FieldMax TO from Coherent, Inc, USA). The geometrical periodicities of LSFL were analyzed using a Scanning Electron Microscope (SEM JSM-7200F of JEOL, Japan)

3. Methods

First, initial single spot experiments with various number of overscans (N_{OS}) and fluence levels (F) at a pulse repetition rate of f=1000Hz at both wavelengths (343nm and 515nm) were conducted to study whether LIPSS form with the given laser system on the samples. The pulse frequency was chosen 1000Hz as this is a typical value used during fs processing of LIPSS on polymers (see Table 2). Table 4 lists an overview of the processing conditions.
Next, the effect of the spatial pulse-to-pulse overlap (OL) on LIPSS formation, when processing a "line" was studied.

4. Results and Discussion

4.1 Results of Single Spot Processing

4.1.1 Polycarbonate (PC)

Similar to pulsed processing, LIPSS occurred after several hundreds to thousand ps laser pulses processing the same spot on both polymer surfaces, when using the conditions listed in Table 4. Fig. 2 shows a part of an ablated crater and its surroundings after processing the PC surface with 1000 pulses at a wavelength of 343nm. One can observe circular concentric rings appear around the ablated crater.

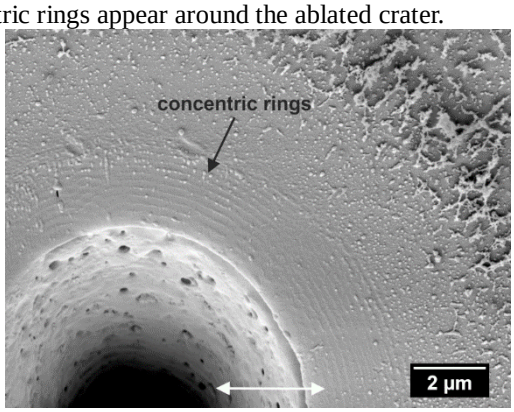

Fig. 2 SEM micrographs showing concentric rings developing around the ablated crater on PC when processing with 1000 pulses of UV laser irradiation at a fluence level of 68mJ/cm^2. The double headed white arrow indicates the direction of E-Field of the laser polarization.

Similar circular concentric rings have been reported on fused silica by Liu et. al. [61]. These authors claimed that the rings origin from the interference of the incident laser beam with the beam which reflects of the slope of the crater. However, the concentric rings found in this study appear around the ablated crater and most probably do not origin from the same physical phenomena. The latter falls out of the scope of this paper.
Additionally, high spatial frequency LIPSS (HSFL) with a periodicity of about 90nm perpendicular to the laser polarization occurred after 1000 pulses at the same fluence level. These HSFL also form around the ablated crater, see Fig. 3.

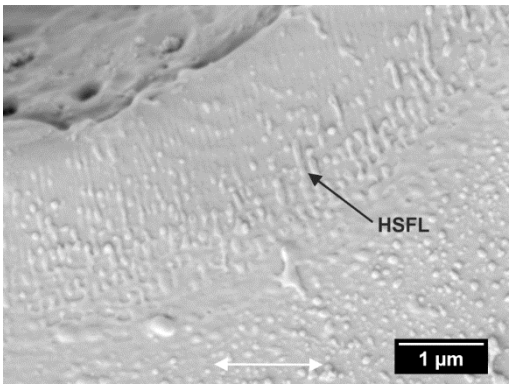

Fig. 3 SEM micrograph of HSFL developing around the ablated crater of PC when processing with 1000 pulses of UV laser irradiation at a fluence of 68mJ/cm^2. The double headed white arrow indicates the direction of E-Field of the laser polarization.

With increasing number of overscans, the circular rings "transformed" to LSFL with a periodicity of about 190nm parallel to the laser polarization, see Fig. 4.

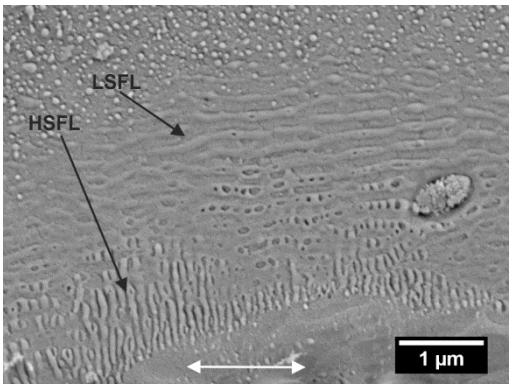

Fig. 4 SEM micrograph of LSFL developing around the ablated crater on PC when processing with 5000 pulses of UV laser irradiation at a fluence of 42mJ/cm^2. The double headed white arrow indicates the direction of E-Field of the laser polarization.

When processing the PC samples with pulses of a wavelength of 515nm, LSFL occur in a ring around the ablated crater with a periodicity of about 370nm after 250 pulses. Similar LSFL can be observed in Fig. 5.
The orientation of the LSFL is concentric with respect to the ablated crater. That is, in this case the orientation of LSFL does not align with the laser polarization direction of the laser light. It is known that for low number of overscans (e.g. NOS=2) LSFL can indeed form independently to the polarization around surface defects, but the orientation shifts to parallel to the laser polarization with only little amount of additional overscans (e.g. NOS=5) [36,41,43]. However, for PC processed with 515nm ps laser pulses, the LSFL orientation stays concentric to the ablated crater even after 1000 pulses, see Fig. 5. After 2000 pulses, the LSFL, which are oriented parallel to the laser polarization, become more pronounced, which can be observed in Fig. 6.

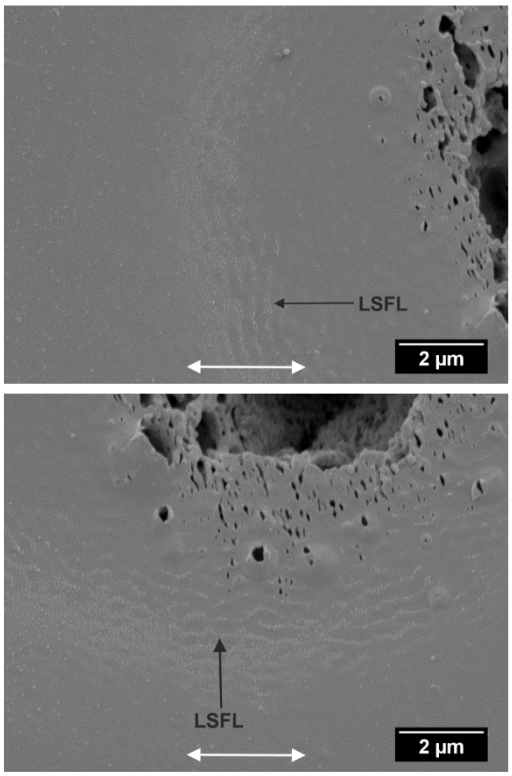

Fig. 5 SEM micrograph of LSFL concentrically oriented around the ablated crater on PC when processing with 1000 pulses of 515nm laser irradiation at a fluence of 100mJ/cm^2. The double headed white arrow indicates the direction of E-Field of the laser polarization. Both micrographs are from the same processed spot. Top: micrograph "left" of the ablated crater; bottom: micrograph "below" the ablated crater.

HSFL with a periodicity of about 70nm perpendicular to the laser polarization occur also after 200 pulses in a ring around the ablated crater, as well as "on top" of the LSFL, se Fig. 6. Like the LSFL parallel to the laser polarization direction, also the HSFL perpendicular to the laser polarization direction become more pronounced with increasing number of overscans, see Fig. 6. The edge of the ablated crater becomes increasingly porous with higher NOS, when processing with 515nm pulses, see Fig. 6.This can be explained by the lower absorptivity of PC at that wavelength. Due to the lower absorptivity at that wavelength, the material absorbs the laser light in deeper regions at material defects which leads to an increase of the temperature in a larger volume when compared with laser pulses of 343nm wavelength. When polymer sheets are produced, typically material of unordered molecule chains will be pressed or rolled in one direction, which aligns the molecule chains in a parallel order. When the material temperature is increased, movement of the polymer chains is more likely in the direction perpendicular to the molecule chain than in the direction along the chain for entropic reasons. Gaseous reaction products due to absorbed laser light gas out through the surface and push the molecule chains apart. This behavior is unfavorable when processing LIPSS, hence, line processing experiments (see section 4.2) were conducted when applying UV wavelength only.

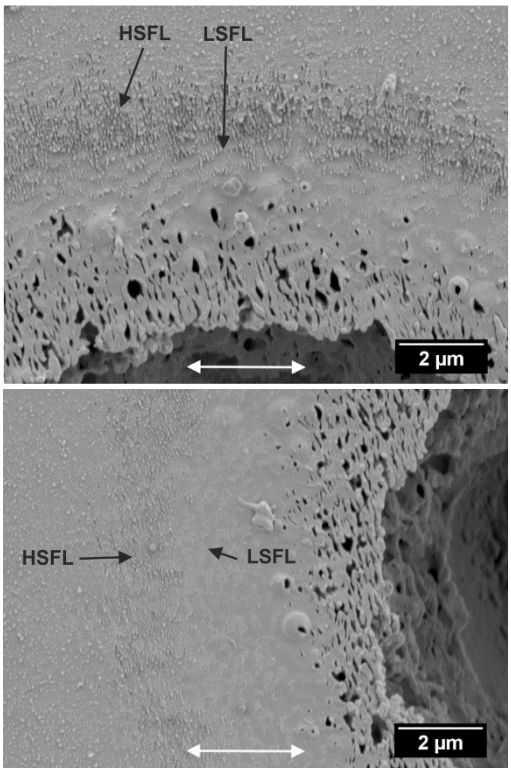

Fig. 6 SEM micrograph of HSFL perpendicular to the laser polarization developing around the ablated crater on PC when processing with 5000 pulses of 515nm laser irradiation at a fluence of 184mJ/cm^2. The double headed white arrow indicates the direction of E-Field of the laser polarization. Both micrographs are from the same processed spot. Top: micrograph "above" the ablated crater; bottom: micrograph "left" of the ablated crater.

4.1.2 Polystyrene (PS)

When processing the PS samples with UV laser pulses, a low number of overscans (N_{OS}<1000) led to either no changes of the surface morphology at fluence levels below the ablation threshold or to ablated craters above the fluence threshold, see Fig. 7. For 1000 pulses, melting occurs around the ablated crater, which smoothens out the rough surface and leads to the possibility of the formation of LIPSS. HSFL with a periodicity of about 50nm develop in the area where melting occurs. Additionally, "lumps" appear in the ablated crater, covered with HSFL with a periodicity of around 70nm, see Fig. 7. Since the PS is a composition of polystyrene and white pigment additives, these additives might show a higher absorptivity then the PS matrix and HSFL form more readily on top of lumped additives.

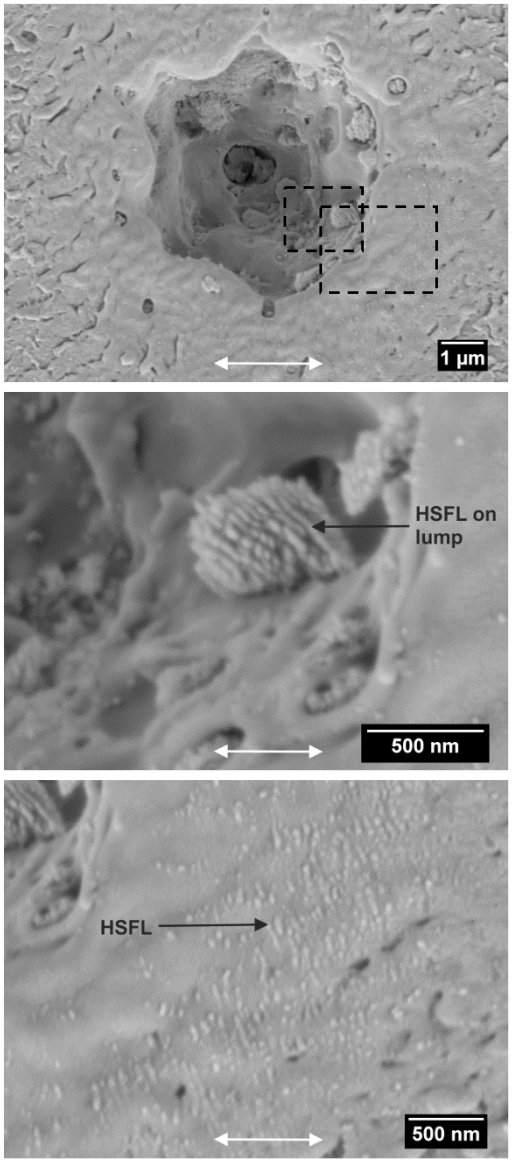

Fig. 7 SEM micrograph of a modified surface area on PS with 1000 pulses of UV laser irradiation at a fluence of 30mJ/cm^2. The boxes in the top micrograph indicate the positions of the excerpts (center and bottom micrograph). HSFL perpendicular to the laser polarization develop around the ablation in the area of melting (bottom). Lumps occur in the ablated crater, covered with HSFL (center). The double headed white arrow indicates the direction of E-Field of the laser polarization.

After 5000 pulses LSFL with a periodicity of around 215nm parallel to the laser polarization can be observed in the area of melting, see Fig. 8.

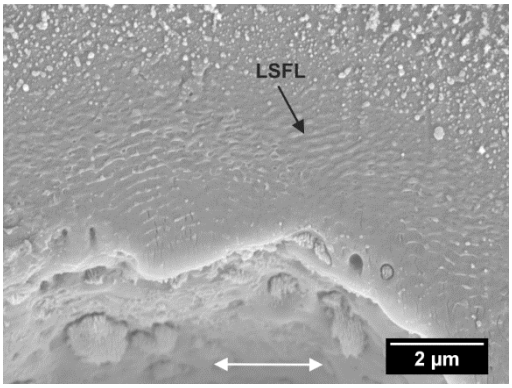

Fig. 8 SEM micrograph of LSFL around ablated crater on PS after 5000 pulses of UV laser irradiation at a fluence of 50mJ/cm². The double headed white arrow indicates the direction of E-Field of the laser polarization.

Processing PS samples with a wavelength of 515nm led to ablation when the fluence level was above the ablation threshold. No ordered structures, nor LIPSS were found.

4.2 Line Processing

From the single spot experiments it can be concluded that several hundreds to thousand pulses are necessary to develop LIPSS on PC and PS in UV. These LIPSS were found around the ablated crater. That implies, a relative high geometrical pulse-to-pulse overlap and high number of overscans are necessary to process a line consisting of homogeneous LIPSS. Here, the overlap is defined by

$$OL = 1 - \frac{v}{d \cdot f} \quad (1)$$

where v is the relative velocity of the focal spot to the surface of the sample, d the diameter of the focused laser spot and f the pulse frequency of the laser source. To achieve similar LIPSS as for single spot laser processing, the pulse frequency was set to f= 1000Hz. The scan velocity was set for an pulse-to-pulse overlap of OL ~ 0.9. The effective number of pulses processing one spot on the surface follows from

$$N_{spot} = N_{OS} \times {}^{d}/_{\Delta x} \quad (2)$$

where Δx is the geometrical distance between laser pulses and can be calculated by $\Delta x = v/f$. The effective number of pulses used for each material are listed in Table 6.

Table 6 Laser scanning conditions and effective number of pulses per spot for processing lines at v=2mm/s, f=1000Hz and d=19.5µm

N_{OS}	N_{spot}
500	4875
1000	9705
2500	24375
5000	48750
7500	73125
10000	97500

4.2.1 Polycarbonate

Fig. 9 shows three SEM micrographs of PC samples processed with 500 overscans with increasing fluence levels. A "low" fluence level of 34mJ/cm² led to increased roughness of the surface, see Fig. 9 (top). At 62mJ/cm² melting occurs in the center of the beam path, as well as holes due to outgassing of gaseous reaction products from photothermal processes, see Fig. 9 (center). Additionally, ablation is visible in the center of the beam path. LSFL with a periodicity of ~290nm parallel to the laser polarization and HSFL with a periodicity of ~100nm perpendicular to the laser polarization appear alongside the melted/ablated area and become more pronounced for higher fluence levels, see Fig. 9 (bottom).

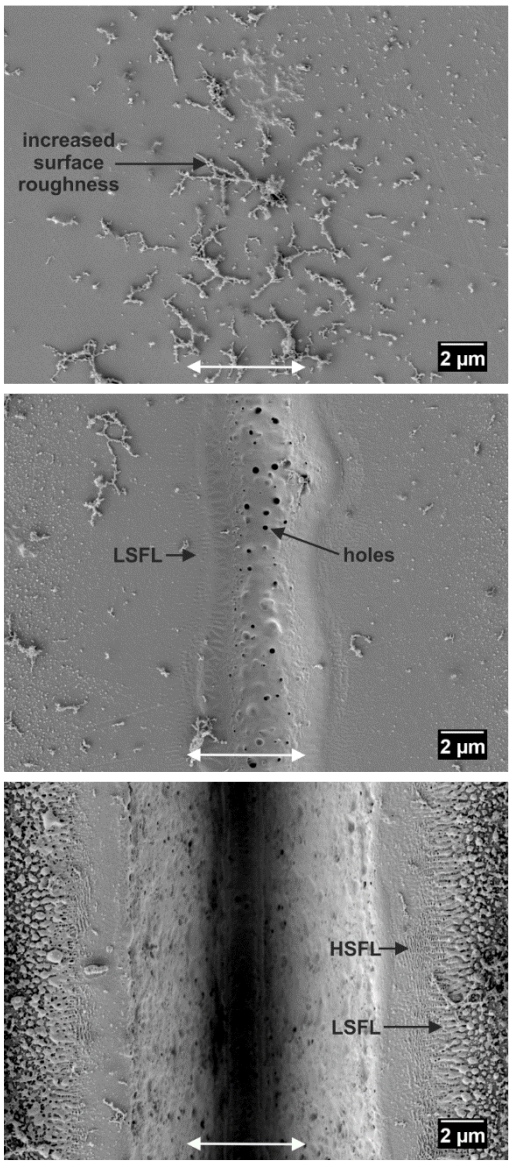

Fig. 9 SEM micrograph of beam path on PC after 500 overscans at a wavelength of 343nm, at fluence levels of 35mJ/cm² (top); 62mJ/cm² (center) and 89mJ/cm² (bottom). The double headed white arrow indicates the direction of E-Field of the laser polarization.

Fig. 10 shows SEM micrographs of PC samples processed with 1000 overscans and a fluence level of 50mJ/cm². The center of the modified area along the beam path consists of LSFL with an average width of around 3µm, spheres and holes in melted areas at the highest fluence level of the Gaussian beam as well as HSFL. HSFL develop predominantly at areas, where melting occurs.

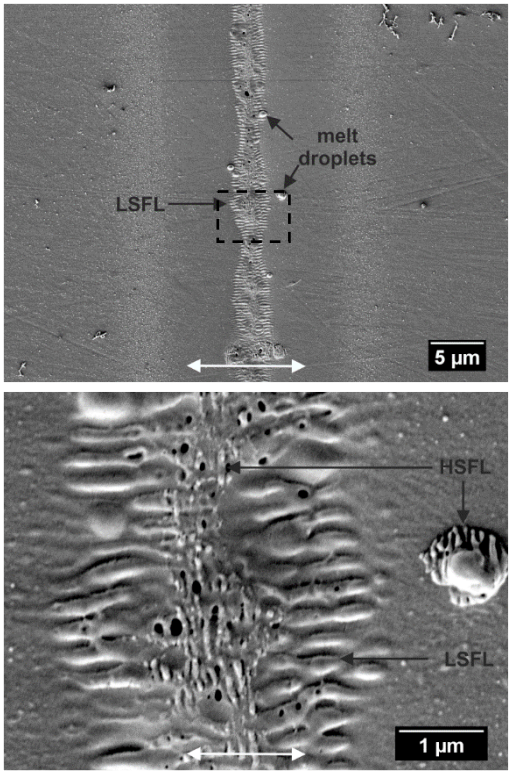

Fig. 10 SEM micrograph of beam path on PC after 1000 overscans at a wavelength of 343nm, at fluence levels of 50mJ/cm^2. The box in the top micrograph indicates the positions of the excerpt (bottom micrograph).The double headed white arrow indicates the direction of E-Field of the laser polarization.

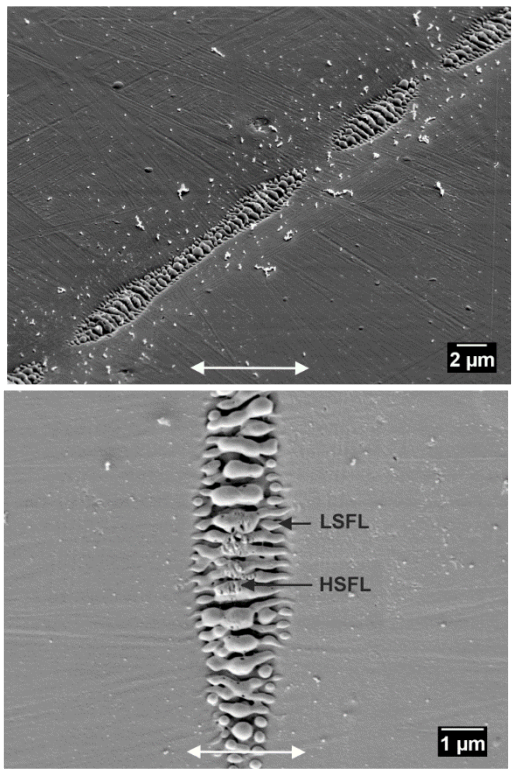

Fig. 11 SEM micrograph of beam path on PC after 5000 overscans at fluence levels of 37mJ/cm^2 taken from a 45° tilted sample. Top image taken at an angle of 45°. The double headed white arrow indicates the direction of E-Field of the laser polarization.

Fig. 11 shows a SEM micrograph of a beam path with 5000 overscans at a fluence of 37mJ/cm^2. The inhomogeneous modified area along the beam path consists only of LSFL with HSFL "on top" in the center of the beam path. Signs of melting were be observed, hence, the accumulated fluence is below the threshold where melting would occur.

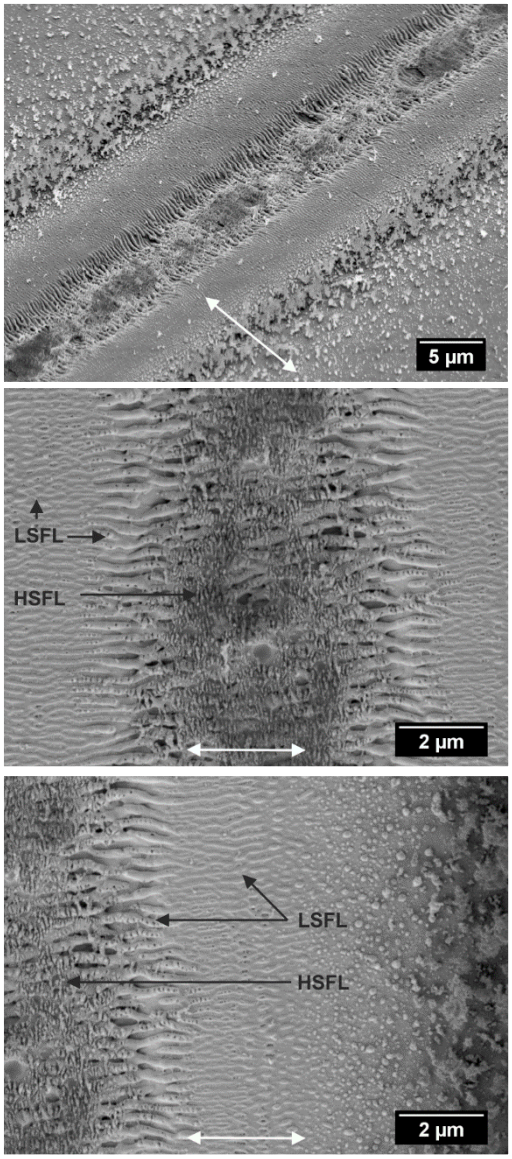

Fig. 12 SEM micrograph of beam path on PC after 7500 overscans at a fluence level of 37mJ/cm^2. Top: sample tilted at 45°; center and bottom: normal to the surface. The double headed white arrow indicates the direction of E-Field of the laser polarization.

An increase of the laser fluence, when applying 5000 overscans leads to a broadening of the effectively processed line along the beam path and therefore to a broadening of structured areas. From the top micrograph in Fig. 12 one can observe two processing regimes. An ablated regime in the center of the beam path and a "non"-ablated, but structured, regime at lower fluence levels of the Gaussian beam profile along the side. LSFL in the ablated regime are broader with a thickness of around 220nm and have a larger periodicity of

around 330nm than the LSFL at the non-ablated regime with a thickness of around 60nm and a periodicity of around 220nm. Additionally, HSFL with a periodicity of around 100nm form on top of LSFL in the ablated areas. From those areas, one can conclude, that the type of LIPSS formation depends on the number of pulses impinging the surface at specific fluence levels, which is also known for metals and semiconductors [62–64]. Hence, at appropriate laser processing conditions it should be possible to process homogeneous areas (overlapping lines) of each type of LIPSS larger than the laser spot. Similar results are achieved at 7500 and 10000 overscans at slightly lower fluence levels.

To investigate the dependency of LIPSS formation regarding the scanning direction, a circle of a diameter of 1mm was processed with 1000 overscans at a fluence level of 34mJ/cm^2. LSFL developed always parallel and HSFL always perpendicular to the laser polarization direction, see Fig. 13.

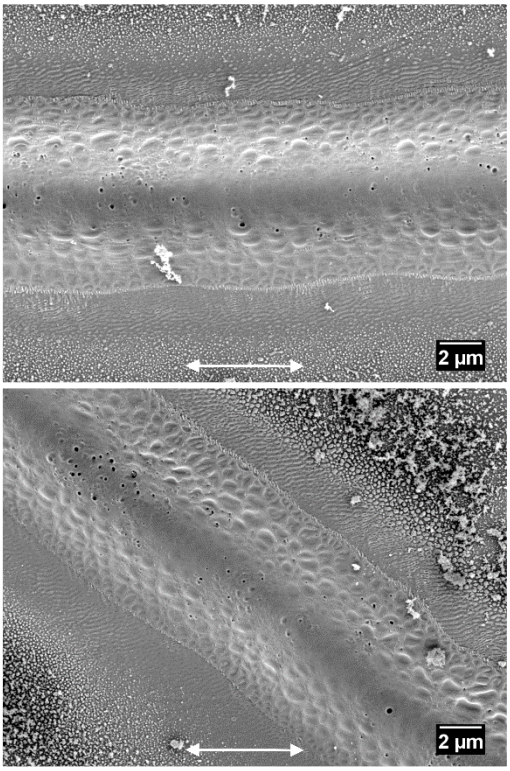

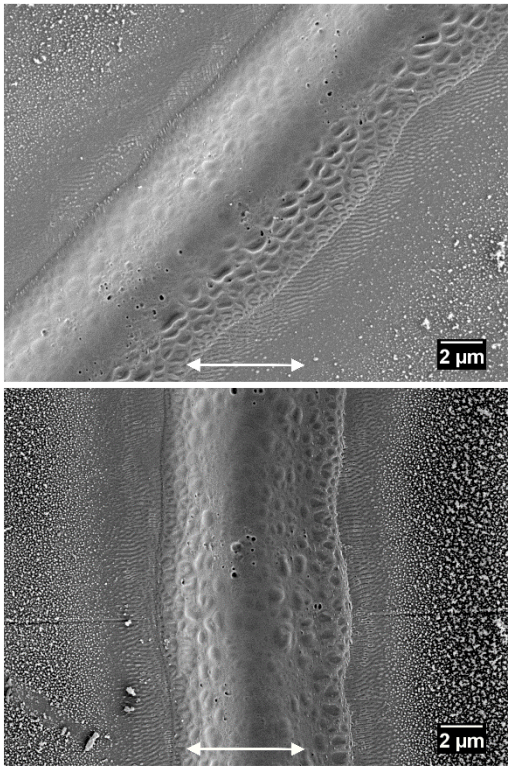

Fig. 13 LSFL and HSFL developing along a circle of 1mm diameter at 1000 overscans and a fluence of 34mJ/cm². The double headed white arrow indicates the direction of E-Field of the laser polarization.

4.2.2 Polystyrene

Processing lines consisting only of LIPSS could not be achieved within the experimental laser processing conditions studied in this paper. That is, when processing within this experimental window, either the sample surface remained unmodified or ablation with modifications alongside of the ablated areas occurred. When ablation occurred, LIPSS develop alongside the ablated line for all studied values of overscans. HSFL with a periodicity of around 100nm appear close to the ablated areas. At lower laser fluence levels, e.g. further away from the ablated regime, LSFL parallel to the laser polarization direction with a periodicity of around 220nm develop alongside the beam path, see Fig. 14 and Fig. 15. Interestingly, LSFL perpendicular to the laser polarization occur randomly at the same fluence regime levels as HSFL, see Fig. 14. These LSFL were observed at overlap values of 500 to 5000 but not for an overlap value of 10000. This phenomena substantiates the conclusions by Pavlov et. al. (see Section 1).

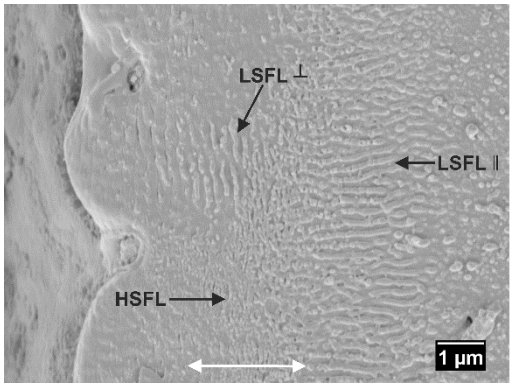

Fig. 14 LIPSS alongside of ablated line on PS at 500 overscans and a fluence of 82mJ/cm². The double headed white arrow indicates the direction of E-Field of the laser polarization.

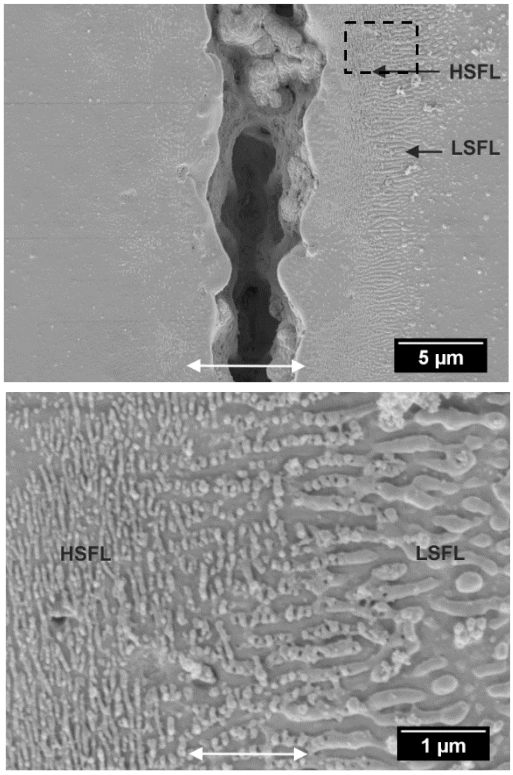

Fig. 15 LIPSS alongside of ablated line on PS at 1000 overscans and a fluence of 73mJ/cm². The box in the top micrograph indicates the positions of the excerpt (bottom micrograph). The double headed white arrow indicates the direction of E-Field of the laser polarization.

4.3. LIPSS on PC and PS processed with ps laser sources compared with fs and ns laser sources

The absorption coefficients of both polymers are negligible, see Table 5, at the studied wavelengths when compared to the absorption coefficients of these polymers when applying the ns and fs laser sources listed in Table 2 and 3. As can be concluded from Table 3, LIPSS were not found when processing polycarbonate using a ns laser source at a wavelength of 248nm, at which the absorptivity of PC is low, but still larger than the absorptivity at the wavelengths studied in this paper (see Table 3). LIPSS have been processed on PC with a fs laser source at a wavelength of 795nm (see Table 2). Rebollar et.al. [29] stated, that the absorption coefficient needs to be high to process LIPSS on polymers with ns laser sources, but when applying fs laser pulses, the absorption coefficient can be lower. In our study, LIPSS were processed on PS and PC at a wavelength of 343nm with a ps laser source. For the studied wavelength of 515nm, LIPSS could only be processed on PC, whereas no ordered structures could be observed on the PS samples. However, at the latter wavelength, ablation craters on PC showed porosity, which indicates heating of the polymer in deeper regions. Thus, this wavelength is not feasible for processing surface structures on polymers, which have a low absorptivity, with ps laser sources. Hence, ps laser sources extend the wavelength spectrum for which processing LIPSS on polymers is possible compared to ns laser sources. However, fs laser sources have a much higher wavelength spectrum, reaching to near infrared, at which LIPSS processing is possible due to two- and multiphoton absorption.

When comparing the number of laser pulses, which are necessary to process LIPSS on PC and PS with ns, ps or fs laser sources, no significant difference can be observed. That is, for all pulse durations several hundred to thousand pulses are necessary to develop LIPSS on these polymers.

Further, for all pulse durations, LSFL processed on PC are parallel to the laser polarization direction. However, when applying ps laser pulses with a wavelength of 343nm led to two types of LSFL depending on the fluence level: below the ablation/melting fluence threshold, normal LSFL were observed with a periodicity of about 220nm. At fluence levels above the melting\ablation threshold, the LSFL periodicity and thickness increased. This phenomenon needs further investigation.

On the other hand, when processing lines on PS applying ps laser pulses with a wavelength of 343nm, led to LSFL parallel and perpendicular to the polarization direction. LSFL perpendicular to the laser polarization direction were found at higher fluence levels, than LSFL oriented parallel to the laser polarization direction.

No HSFL structures have been reported yet on PS or PC, when ns or fs laser pulses were applied. Nonetheless, HSFL have been reported on PET [18,37] and on PLLA [65] when applying fs laser pulses. When applying ps laser pulses on PS and PC samples, HSFL were observed, predominantly at melted or ablated areas.

5. Summary

Based on a literature review it was concluded that, so far, the formation of Laser-induced Periodic Surface Structures (LIPSS) on polymers was only studied when applying laser sources operating either in the UV wavelength and nanosecond pulse duration, or radiation of wavelengths ranging from 265nm to 1045nm and pulse durations in the femtosecond regime. Also, High Spatial Frequency LIPSS (HSFL) have only been reported when processing polymers with fs laser sources. In this study, two polymers were irradiated with two wavelengths (343nm and 515nm), using a laser source with a pulse duration in the picosecond regime. Single spot and line processing experiments were conducted to study LIPSS formation on polystyrene (PS) and polycarbonate (PC). It

was found that Low Spatial Frequency LIPSS (LSFL) and HSFL do form on PC and PS at a wavelength of 343nm. Moreover, it can be concluded from the line processing experiments, that processing homogenous areas of either LSFL or HSFL on PC can be achieved by using appropriate laser processing conditions. That is, by applying a high number of pulses impinging one spot at laser fluence levels below the melting threshold. LIPSS were also achieved on PS during line processing experiments, however, only alongside of ablated areas. At a wavelength of 515nm, LSFL and HSFL do form on PC, but the processed surface does become porous when applying that wavelength. LIPSS were not found on PS at the latter wavelength. Hence, ps laser sources have a broader wavelength spectra, at which LIPSS processing is possible, than ns laser sources but do not reach the wavelength spectra of fs laser pulses for allowed LIPSS development.

References

[1] Y. Jin, O. J. Allegre, W. Perrie, K. Abrams, J. Ouyang, E. Fearon, S. P. Edwardson, and G. Dearden: Opt. Express, 21, (2013) 25333.

[2] J. Bonse, J. Krüger, S. Höhm, and A. Rosenfeld: J. Laser Appl., 24, (2012) 042006.

[3] J. Vincenc Obona, V. Ocelík, J. Z. P. Skolski, V. S. Mitko, G. R. B. E. Römer, A. J. Huis In't Veld, and J. T. M. De Hosson: Appl. Surf. Sci., 258, (2011) 1555.

[4] F. Preusch, S. Rung, and R. Hellmann: J. Laser Micro/Nanoengineering, 11, (2016) 137.

[5] J. Romano, A. Garcia-giron, P. Penchev, and S. Dimov: Appl. Surf. Sci., 440, (2018) 162.

[6] M. Birnbaum: J. Appl. Phys., 36, (1965) 3688.

[7] P. M. Fauchet and A. E. Siegman: Appl. Phys. Lett., 40, (1982) 824.

[8] J. Bonse, K. W. Brzezinka, and A. J. Meixner: Appl. Surf. Sci., 221, (2004) 215.

[9] T. Baldacchini, J. E. Carey, M. Zhou, and E. Mazur: Langmuir, 22, (2006) 4917.

[10] J. Eichstät, G. R. B. E. Römer, and A. J. Huis in't Veld: Phys. Procedia, 12, (2011) 7.

[11] P. A. Temple and M. J. Soileau: IEEE J. Quantum Electron., 17, (1981) 2067.

[12] Y. Liu, Y. Brelet, Z. He, L. Yu, S. Mitryukovskiy, A. Houard, B. Forestier, A. Couairon, and A. Mysyrowicz: Phys. Rev. Lett., 110, (2013) 1.

[13] S. Höhm, M. Herzlieb, A. Rosenfeld, J. Krüger, and J. Bonse: Appl. Surf. Sci., 374, (2016) 331.

[14] N. Yasumaru, K. Miyazaki, and J. Kiuchi: Appl. Phys. A Mater. Sci. Process., 76, (2003) 983.

[15] P. E. Dyer and R. J. Farley: Appl. Phys. Lett., 57, (1990) 765.

[16] M. Bolle and S. Lazare: Appl. Surf. Sci., 65–66, (1993) 349.

[17] M. Bolle and S. Lazare: J. Appl. Phys., 73, (1993) 3516.

[18] J. Heitz, E. Arenholz, D. Bäuerle, R. Sauerbrey, and H. M. Phillips: Appl. Phys. A Solids Surfaces, 59, (1994) 289.

[19] M. Csete and Z. Bor: Appl. Surf. Sci., 133, (1998) 5.

[20] E. Rebollar, M. Castillejo, and T. A. Ezquerra: Eur. Polym. J., 73, (2015) 162.

[21] J. Cui, A. Nogales, T. A. Ezquerra, and E. Rebollar: Appl. Surf. Sci., 394, (2017) 125.

[22] O. Neděla, P. Slepička, P.Sajdl, M. Veselý, and V. Švorčík: Surf. Interface Anal., 49, (2017) 25.

[23] J. Bonse, S. Höhm, S. V. Kirner, A. Rosenfeld, and J. Krüger: IEEE J. Sel. Top. Quantum Electron., 23, (2017) 9000615.

[24] M. Groenendijk: Laser Tech. J., 5, (2008) 44.

[25] J. Bonse, M. Munz, and H. Sturm: J. Appl. Phys., 97, (2005) 013538.

[26] J. F. Young, J. E. Sipe, and H. M. Van Driel: Phys. Rev. B, 30, (1984) 2001.

[27] E. Rebollar, I. Frischauf, M. Olbrich, T. Peterbauer, S. Hering, J. Preiner, P. Hinterdorfer, C. Romanin, and J. Heitz: Biomaterials, 29, (2008) 1796.

[28] E. Rebollar, S. Pérez, M. Hernández, C. Domingo, M. Martín, T. a Ezquerra, J. P. García-Ruiz, and M. Castillejo: Phys. Chem. Chem. Phys., 16, (2014) 17551.

[29] E. Rebollar, M. Castillejo, and T. A. Ezquerra: Eur. Polym. J., 73, (2015) 162.

[30] E. Rebollar, M. Sanz, S. Pérez, M. Hernández, I. Martín-Fabiani, D. R. Rueda, T. a Ezquerra, C. Domingo, and M. Castillejo: Phys. Chem. Chem. Phys., 14, (2012) 15699.

[31] E. Rebollar, M. Hernández, M. Sanz, S. Pérez, T. A. Ezquerra, and M. Castillejo: J. Appl. Polym. Sci., 132, (2015) 2.

[32] A. Rodríguez-Rodríguez, E. Rebollar, M. Soccio, T. A. Ezquerra, D. R. Rueda, J. V. Garcia-Ramos, M. Castillejo, and M. C. Garcia-Gutierrez: Macromolecules, 48, (2015) 4024.

[33] D. E. Martínez-Tong, Á. Rodríguez-Rodríguez, A. Nogales, M. C. García-Gutiérrez, F. Pérez-Murano, J. Llobet, T. A. Ezquerra, and E. Rebollar: ACS Appl. Mater. Interfaces, 7, (2015) 19611.

[34] I. Pavlov, O. Yavuz, G. Makey, O. Toke, and O. Ilday: arXiv:1710.11405v1, (2017) 1.

[35] E. Rebollar, J. R. Vázquez de Aldana, I. Martín-Fabiani, M. Hernández, D. R. Rueda, T. A. Ezquerra, C. Domingo, P. Moreno, and M. Castillejo: Phys. Chem. Chem. Phys., 15, (2013) 11287.

[36] M. Forster, W. Kautek, N. Faure, E. Audouard, and R. Stoian: Phys. Chem. Chem. Phys. Phys. Chem. Chem. Phys, 13, (2011) 4155.

[37] J. Heitz, B. Reisinger, M. Fahrner, C. Romanin, J. Siegel, and V. Svorcik: Int. Conf. Transparent Opt. Networks, (2012) 1.

[38] E. Rebollar, J. R. Vázquez De Aldana, J. A. Pérez-Hernández, T. A. Ezquerra, P. Moreno, and M. Castillejo: Appl. Phys. Lett., 100, (2012) 041106.

[39] M. Castillejo, T. A. Ezquerra, M. Martín, M. Oujja, S. Pérez, and E. Rebollar: AIP Conf. Proc., 1464, (2012) 372.

[40] Y. Sato, M. Tsukamoto, T. Shinonaga, and T. Kawa: Appl. Phys. A Mater. Sci. Process., 122, (2016) 1.

[41] S. Baudach, J. Kruger, and W. Kautek: Laser Rev., 29, (2001) 705.

[42] E. Yousif and R. Haddad: Springerplus, 2, (2013)

398.
[43] M. Csete, O. Marti, and Z. Bor: Appl. Phys. A Mater. Sci. Process., 526, (2001) 521.
[44] M. Csete, R. Eberle, M. Pietralla, O. Marti, and Z. Bor: Appl. Surf. Sci., 208–209, (2003) 474.
[45] M. Csete, S. Hild, A. Plettl, P. Ziemann, Z. Bor, and O. Marti: Thin Solid Films, 453–454, (2004) 114.
[46] U. Prendergast, S. Kudzma, R. Sherlock, C. O'Connell, and T. Glynn: Proc. SPIE, 6458, (2007) 64581V.
[47] P. Slepička, E. Rebollar, J. Heitz, and V. Švorčík: Appl. Surf. Sci., 254, (2008) 3585.
[48] J. Siegel, P. Slepička, J. Heitz, Z. Kolská, P. Sajdl, and V. Švorčík: Appl. Surf. Sci., 256, (2010) 2205.
[49] J. Heitz, R. A. Barb, C. Hrelescu, J. Siegel, P. Slepicka, V. Vosmanska, V. Svorcik, B. Magnus, and R. Marksteiner: Int. Conf. Transparent Opt. Networks, (2014) 295.
[50] W. Pfleging, M. Bruns, A. Welle, and S. Wilson: Appl. Surf. Sci., 253, (2007) 9177.
[51] I. Martín-Fabiani, E. Rebollar, S. Pérez, D. R. Rueda, M. C. García-Gutiérrez, A. Szymczyk, Z. Roslaniec, M. Castillejo, and T. A. Ezquerra: Langmuir, 28, (2012) 7938.
[52] E. Rebollar, D. R. Rueda, I. Martín-Fabiani, Á. Rodríguez-Rodríguez, M. C. García-Gutiérrez, G. Portale, M. Castillejo, and T. A. Ezquerra: Langmuir, 31, (2015) 3973.
[53] J. E. Sipe, J. F. Young, J. S. Preston, and H. M. Van Driel: Phys. Rev. B, 27, (1983) 1141.
[54] J. Bonse, S. Höhm, S. Kirner, A. Rosenfeld, and J. Krüger: Conf. Lasers Electro-Optics, 23, (2016) 9000615.
[55] J. Reif, O. Varlamova, S. Uhlig, S. Varlamov, and M. Bestehorn: Appl. Phys. A Mater. Sci. Process., 117, (2014) 179.
[56] A. Borowiec and H. K. Haugen: Appl. Phys. Lett., 82, (2003) 4462.
[57] X.-F. Li, C.-Y. Zhang, H. Li, Q.-F. Dai, S. Lan, and S.-L. Tie: Opt. Express, 22, (2014) 28086.
[58] X. Sedao, M. V. Shugaev, C. Wu, T. Douillard, C. Esnouf, C. Maurice, S. Reynaud, F. Pigeon, F. Garrelie, L. V. Zhigilei, and J. P. Colombier: ACS Nano, 10, (2016) 6995.
[59] M. D. Migahed and H. M. Zidan: Curr. Appl. Phys., 6, (2006) 91.
[60] R. G. Kadhim: World Sci. News, 30, (2016) 14.
[61] Y. Liu, Y. Brelet, Z. He, L. Yu, B. Forestier, Y. Deng, H. Jiang, and A. Houard: Appl. Phys. Lett., 102, (2013) 251103.
[62] J. Lehr and A. M. Kietzig: Opt. Lasers Eng., 57, (2014) 121.
[63] K. M. T. Ahmmed, E. J. Y. Ling, P. Servio, and A. M. Kietzig: Opt. Lasers Eng., 66, (2015) 258.
[64] J. Eichstädt and A. J. Huis In't Veld: Phys. Procedia, 41, (2013) 650.
[65] S. Yada and M. Terakawa: Opt. Express, 23, (2015) 5694.

(Received: June 24, 2018, Accepted: September 12, 2018)